

Surface investigation and catalytic activity of iron-modified TiO₂

Somayeh Sohrabi¹ · Faranak Akhlaghian¹

Received: 23 September 2015 / Accepted: 2 November 2015 / Published online: 23 November 2015
© The Author(s) 2015. This article is published with open access at Springerlink.com

Abstract Iron-modified titanium dioxide nanostructured catalyst was synthesized by sol–gel method. Due to the important impacts of surface properties on the catalytic activity, the catalyst surface is investigated. To have a complete characterization of the catalyst, TEM, SEM, XPS, XRF, XRD, BET, and TGA–DTA techniques were used. XRF analysis reveals the iron loading of the synthesized catalyst as Fe₂O₃/TiO₂ = 0.21 %. XRD results imply that the catalyst is composed of anatase and rutile phases. The SEM image indicates the mesoporousity of the nanoparticles. Clusters are observable in the TEM images. The main objective of activity tests is focused upon the comparative evaluation of H₂O₂ addition and the application of air bubbling. Experimental results specified that the optimum amount for H₂O₂ dosage is 12.5 ml. Moreover, it has been observed that an increase in the aeration flow rate shows a positive effect on the degradation of phenol and the optimum aeration flow is 9 l/min. Furthermore, it has been shown that the addition of copper as additive ion to phenol solution boosts the degradation of phenol; the highest phenol degradation efficiency after 120 min (43.85 %) was attained under this condition.

Keywords Surface characterization · Iron-modified titanium dioxide · Catalyst · Dopant

Background

All solid materials interact with their surroundings through their surfaces. The characteristics of these interactions are defined by the physical properties and chemical composition of the surfaces. The surface chemistry affects important properties of the solid such as the corrosion rates, catalytic activity, adhesive properties, wettability, contact potential, and failure mechanisms. It has been proven that the catalytic activity of a catalyst depends not only on chemical components, but also on the particles dimension, morphology, and structural properties of the catalyst. Moreover, the catalyst preparation method has a great impact on the particle properties and the dispersion state of the active components. Different preparation methods such as incipient wetness impregnation, co-precipitation, hydrothermal synthesis, and sol–gel method are often used to obtain the catalysts with different physicochemical properties. The preparation method has a significant role in improving the activity of catalysts [1–3]. TiO₂, which is used in the decomposition of organics, is one of the most efficient photocatalysts that acts in the ambient conditions. Moreover, TiO₂ is considerably available, inexpensive, non-toxic, and it is reputed for its high chemical stability [3]. TiO₂ has various applications in fields of hydrogen production, antibacterial activity, air cleaning and water treatment processes, and it has been applied for the decomposition of a large number of organic pollutants. The application of TiO₂ in degradation of pollutants is considered as a promising technique in the wastewater industry [4]. Loghman Karimi and Salar Zohoori synthesized TiO₂/SrTiO₃ nanocomposite and evaluated its photocatalytic activity by the degradation of azo dyes. On the composite system, strontium titanate plays the role of electron acceptor to accelerate photodecomposition [5]. Numerous

✉ Somayeh Sohrabi
sohrabisomayeh@yahoo.com; s.sohrabi@eng.uok.ac.ir

¹ Department of Chemical Engineering, Faculty of Engineering, University of Kurdistan, Sanandaj, Iran

research projects have focused on the surface modification of TiO_2 , the most commonly employed modification method is loading nano-sized metals on TiO_2 surface. Dopants are used to retard the fast charge recombination and enhance the interfacial charge transfer [6]. Metallic nanoparticles such as Pt [7], Pd [8], Au [9], Ag [10–14], Ru [15], and Fe [16–20] have been used to enhance the photocatalytic activity of TiO_2 by decelerating the recombination behaviors. The photo-induced electrons migrate to the metal due to the relatively low Fermi level of metals, which make the photo-induced holes stable on the TiO_2 surface and contributes to the charge separation [3, 21, 22]. Therefore, more OH radicals are generated as an enhanced redox reaction [4].

The following is a summary of research papers that are typically associated with the modification of TiO_2 with Fe. Oganisian et al. [23] studied the influence of Fe ions on the magnetic properties of TiO_2 . The magnetization as a function of temperature and applied magnetic field of TiO_2 nanopowders doped with 1, 5 and 10 mol% Fe and prepared by sol–gel method in two different ways has been measured in the wide temperature and magnetic field range. Except for the low Fe fraction samples, all compounds exhibit the paramagnetic behavior with the negative Curie temperature that suggests the antiferromagnetic ordering. The measurements showed that magnetic properties are more related to the nanopowders preparation method than to their grain size [23]. Hreniak et al. [24] investigated the optical properties of iron-modified titanium dioxide. Titanium dioxide nanoparticles with different amount of Fe were synthesized by a sol–gel method. The zeta potential analysis indicates that existence of iron changed the zeta potentials of titanium dioxide. Magnetic force microscopy study illustrates the ferromagnetic nature of observed particles. The SEM images confirm the nanostructure of the catalysts [24]. Ranjit and Viswanathan [25] showed that doping TiO_2 with Fe(III) enhances its photocatalytic activity. They ascribed the improved photocatalytic activity of the iron-doped catalysts to the heterojunction formed between the Fe/TiO_2 and $\alpha\text{-Fe}_2\text{O}_3$ phases for the sol–gel-derived catalysts [25]. Liu et al. [26] prepared the Fe-doped TiO_2 nanorod clusters and monodispersed nanoparticles by a modified hydrothermal and solvothermal method. The Fe^{3+} dopants in TiO_2 lattices not only lead to the significantly extending of the optical responses from UV to visible region, but also diminish the recombination rates of the electrons and holes. The photocatalytic activities were evaluated by photocatalytic decomposition of formaldehyde in air under visible light illumination. Compared with P25 (TiO_2) and N-doped TiO_2 nanoparticles, the Fe-doped photocatalysts show high photocatalytic activities under visible light [26]. Naik and Parida [27] Prepared and characterized mesoporous

$\text{Fe}_x\text{Ti}_{1-x}\text{O}_{2-y}\text{N}_y$ nanophotocatalyst (FeNT). They demonstrated that the presence of Fe ion facilitates the surface charge transfer and noted that the synergistic effect of iron and nitrogen greatly enhances the photocatalytic activity [27]. Barakat et al. [28] investigated $\text{ZnO-Fe}_2\text{O}_3$ incorporated TiO_2 nanofibers as a photocatalyst for water splitting under visible light radiation. The band gap energy of titanium oxide nanofibers was modified by Fe_2O_3 and ZnO incorporation to be used as effective photocatalysts in water splitting process under visible light radiation [28].

The main goal of this study is optimizing H_2O_2 dosage, air bubbling, temperature, and additive ions on the photocatalysis using iron-modified titanium dioxide. The other objective of this work is the study of the surface of the catalyst and our focus is on the surface composition, structure, and morphology of Fe/TiO_2 . Sol–gel method was chosen because the stoichiometry of the proposed process is controllable and the powders, which are synthesized by this method, are highly pure and the required equipment is inexpensive.

Methods

Material and method

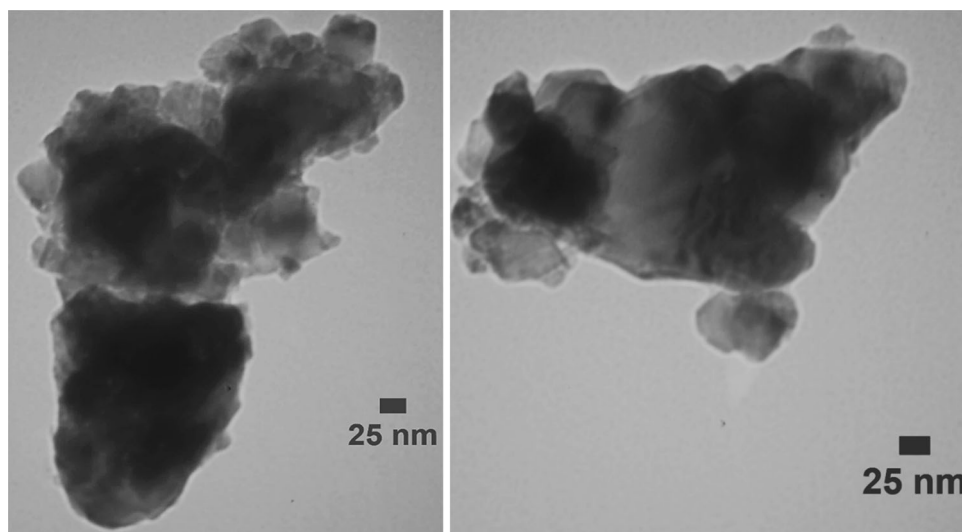
Titanium isopropoxide (98 %) and $\text{Fe}(\text{NO}_3)_3 \cdot 9\text{H}_2\text{O}$ (98 %) were used as the precursors for the titanium and iron, respectively. Moreover, ethanol (96 %), nitric acid (65 %), H_2O_2 (30 %) and phenol (99 %) were used in the experiments. All the materials were purchased from Merck Company. The materials were of analytical grade and were used without further purifications.

Following Yoldas method, titanium isopropoxide was added to double-distilled water. The molar ratio of titanium isopropoxide to water was 1:100. The mixture was stirred at a constant rate and heated until the temperature reached 85 °C. Then nitric acid was added. The molar ratio of titanium isopropoxide to nitric acid was 1:0.07. Fe was added to the mixture through the solution, which is obtained by dissolving $\text{Fe}(\text{NO}_3)_3 \cdot 9\text{H}_2\text{O}$ in ethanol. The mixture was under reflux at 85 °C for 24 h. The obtained gel was dried at 100 °C in an oven. Then, the calcination process had been taken place in a furnace at 600 °C for 2 h [29]. Finally, Fe/TiO_2 was crushed and sieved into 60–90 μm .

Characterization techniques

Surface morphology of the catalyst was investigated by SEM of TSCAN company on 25.0 kV acceleration voltage and TEM analyze was performed by transmission electron microscope of Zeiss company operated at acceleration

Fig. 1 TEM images of images of iron-modified titanium dioxide



voltage of 80 kV. An important step in characterizing the surface chemistry of the specimen is to identify the elements present on the surface. To achieve this, we used X-ray photoelectron spectroscopy (XPS: TWIN ANODE XR3E2 X-RAY SOURCE SYSTEMS, X-RAY 8025-Bes-Tec) and recorded a survey spectrum over the region of 0–1200 eV that provided fairly strong peaks for all elements in the periodic table. The data were presented as a graph of intensity versus electron energy. Iron content of the catalyst was measured by SPECTRO X-labPro X-ray fluorescence (XRF) spectrometer. The XRD pattern was collected using X'Pert MPD diffractometer of the Philips company (the Netherlands) with Cu $K\alpha$ radiation at 40 kV and 40 mA at a scan rate of 0.2 °/s over 2θ range of 5°–80°. Specific surface area (BET) of the sample was measured using an ASAP Micrometrics 2011. The TGA–DTA analysis of the Fe/TiO₂ catalyst was carried out in a TGA analyzer ATA PT1000 model of the Linseis Company under static air atmosphere in the temperature range of 33.5–650 °C.

Results and discussions

Characterization

TEM images of the catalyst are shown in Fig. 1. It can be observed that particles tend to agglomerate at dimensions near 250 nm. The structure and morphology of the catalyst were investigated by Scanning Electron Microscopy. SEM image of the catalyst is depicted in Fig. 2. Porous structure of the catalyst is revealed in this nanoscale image.

Figure 3 shows the typical XPS survey scan of the Fe/TiO₂ sample. No iron could be detected in the surface of sample, which could be because of low concentration of

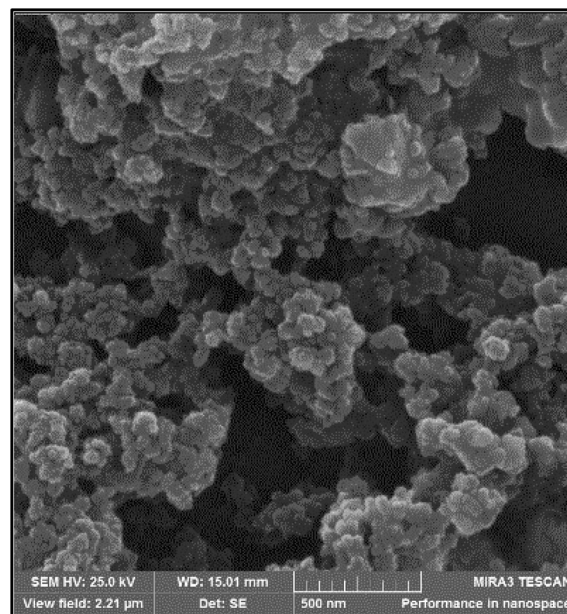


Fig. 2 SEM image of iron-modified titanium dioxide

iron being dopant. TiO₂ rutile structure has open diffusion channels with a radius of ~ 0.77 Å that run parallel to the c -axis [30]. Since the radius of Fe³⁺ is 0.64 Å, which is smaller than both the 0.77 Å channels in the porous structure of pure TiO₂ and the radius of Ti⁴⁺ (0.68 Å) [31, 32], it is possible that Fe³⁺ diffuses along the c -axis and substitutes Ti⁴⁺ in the TiO₂ lattice [31]. Figure 3a, b show the high-resolution XPS spectra of titanium and oxygen. From Fig. 3a, it is clear that there are four contributions to the Ti 2*p* region: the Ti (2*p*3/2) and Ti (2*p*1/2) at binding energies of 458.8 and 464.4 eV, respectively. These values for binding energies are in agreement with the values relevant to TiO₂, moreover, the difference between these two

XPS spectra of Fe/TiO₂

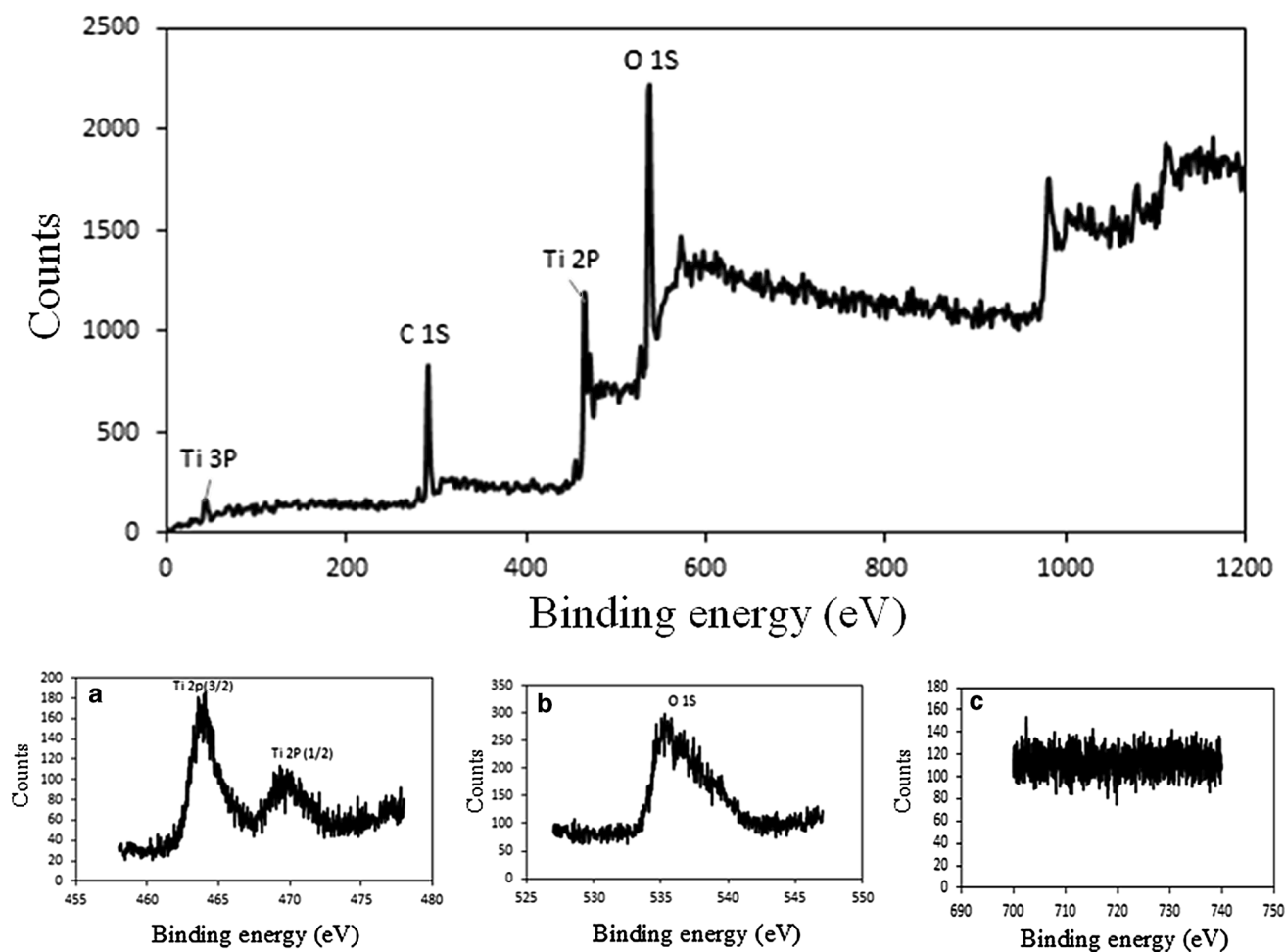


Fig. 3 XPS survey scan of the Fe/TiO₂ sample. **a** XPS spectra of titanium, **b** XPS spectra of oxygen, **c** XPS resolution spectrum of Fe

binding energies represents the standard binding energy for Ti element [33]. Upon substitution of Ti⁴⁺ with Fe³⁺, the number of electrons of the conduction band of TiO₂ is increased, this bring about the migration of these electrons to iron which results in a decrease in the outer electron cloud density of Ti ions, and overall, It leads to the corresponding increase in generation of surface state of Ti³⁺. Hence, the existence of the Ti³⁺ means the presence of Fe³⁺. Existence of Ti³⁺ will retard the recombination of the h⁺ and e⁻, which has a positive effect on the catalytic activity of Fe/TiO₂ [34, 35]. Figure 3b shows the corresponding spectra of oxygen with the following composition: The main contribution of oxygen in the Fe/TiO₂ is composed of O²⁻ (58.1 %), which can be assigned to the oxygen bounded in the TiO₂ lattice (Ti–O). Its peak is corresponded to binding energy of 530.10 eV. Moreover, 16.6 % of the total oxygen is associated with O⁻ which is indicated the presence of surface hydroxyl groups (Ti–OH) as chemisorbed water, The relevant peak is located around

531.8 eV and finally 25.3 % is in the form of physically absorbed water, pertaining to the peak at 533.4 eV [34, 35]. Figure 3c indicates that iron concentration is below the detection level of XPS. The enhanced activity of Fe/TiO₂ compared with TiO₂ is experimentally shown in Fig. 4, which confirms that Fe³⁺ ions are absorbed on the TiO₂ surface, acting as electron trapping centers. Thus, they increase the electron–hole pair separation efficiency and accordingly, superior activity of Fe/TiO₂ confirms the presence of iron in the surface of the photocatalyst.

The results of XRF analysis for the catalyst characterization are presented in Table 1. Chemical composition of the synthesized catalyst reveals that it is consisted of TiO₂ (95.85 %), Fe₂O₃ (0.20 %) and Na₂O (0.42 %), Al₂O₃ (0.69 %), SiO₂ (2.84 %) and the ratio of (Fe₂O₃/TiO₂) is (0.2 %/95.85 % = 0.21 %).

XRD pattern of the catalyst is shown in Fig. 5. Peaks at 32.0095°, 42.1696° and 64.0611° are attributed to the rutile phase (JCPDS File no. 21-1276) and the peak at 29.5090°

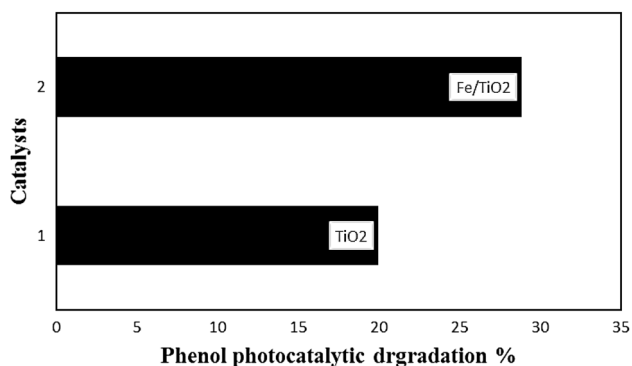


Fig. 4 The effect of Fe photocatalytic activity of the catalyst (Initial phenol concentration: 200 ppm, catalyst loading: 0.5 g/l, H₂O₂: 12.5 ml, 30 wt%, reaction time: 120 min, UV light intensity of 757.38 mW/cm²)

Table 1 Chemical composition of the catalyst

Z	Symbol	Element	Concentration (%)
22	TiO ₂	Titanium	95.85
26	Fe ₂ O ₃	Iron	0.20
11	Na ₂ O	Sodium	0.42
13	Al ₂ O ₃	Aluminum	0.69
14	SiO ₂	Silicon	2.84

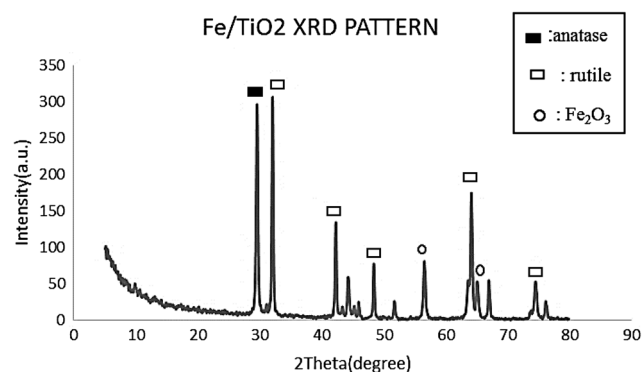


Fig. 5 XRD pattern of Fe/TiO₂

is attributed to the anatase phase (ICPDS File no. 21-1272). These results imply that both rutile and anatase phases exist in the catalyst. In addition to the peaks belonging to rutile and anatase phases other peaks are also recognized which correspond to iron oxides of Fe₂O₃ (JCPDS File no. 39-1346). It confirms the existence of iron as dopant in the sample and proves that iron is in its oxide form.

BET model, which was developed by Brunauer, Emmet and Teller is applied for measuring the surface of the catalyst. Based on the IUPAC classification, porous structures are categorized based on their pore sizes, micro pores (pores with diameters less than 2 nm), mesopores (pores

with 2–50 nm diameter), and macropores (pores with diameters greater than 50 nm) [36]. Since the average pore diameter of Fe/TiO₂ (4 V/A by BET) is 13.9838 nm, the catalyst is considered mesoporous, according to IUPAC classification and specific surface area of the catalyst is 5.1268 m²/g. Pore size distribution is multimodal and the decreased prevalence of the pores with increased pore size is evident in Fig. 6.

Figure 7 shows the thermal gravimetric analysis (TGA) and differential thermal analysis (DTA) of Fe/TiO₂ catalyst. In TGA curve, three regions with different slopes are recognized. These regions are 33.5–200.6, 200.6–416.5, and 416.5–650 °C, respectively. In the first region, weight loss is attributed to the vaporization of water and the degradation of volatile organic materials. In the second region, 200.6–416.5 °C, decomposition of the organic materials with strong bond has occurred. Weight loss in the third region, 416.5–600 °C, is negligible and insignificant. In DTA curve, an endothermic broad peak around 100 °C is observed which is attributed to the vaporization of water. The following two exothermic peaks around 200 °C are attributed to the combustion of organics. The broad exothermic peak with onset of 400 °C is representative of the crystallization process. It is notable that below this temperature, the material is amorphous; at 400 °C crystallization begins with the formation of anatase followed by phase transformation from anatase to rutile. The results show excellent agreement with the work of Mesgari et al. [37].

Activity tests

The photocatalytic activity of Fe-doped TiO₂ nanoparticles was examined by studying the degradation of phenol. A specified amount of the synthesized catalyst (0.5 g/l) was added to the phenol solution (200 ppm, 200 ml), which was selected as the synthetic wastewater. The amount of Fe-loading of Fe/TiO₂ catalyst, initial phenol concentration, and catalyst dosage were investigated and optimized in our previous work [38]. Hydrogen peroxide (H₂O₂: 30 wt%) was added to the solution as an oxidizing agent. The mixture was stirred at a constant rate and illuminated by the UV lamp (with light intensity of 757.38 mW/cm²) which was fixed 19.5 cm above the batch reactor (Pyrex vessel capacity: 2 l). In this work, air bubbling is carried out by two parallel air pumps. One RS Electrical (model: RS-610) with the maximum flow of 3.5 l/min and the other is HAILEA (model: ACO-5505), with maximum flow is 5.5 l/min. The setup was shielded by aluminum foil during the reaction time to prevent the interference with outside light. After 2 h of reaction, the mixture was centrifuged and the absorbance of the supernatant solution was measured at 270 nm using a Specord 210 UV spectrometer. The experiments were repeated for the blank. All the



Fig. 6 Pore size distribution according to BJH adsorption of Fe/TiO₂

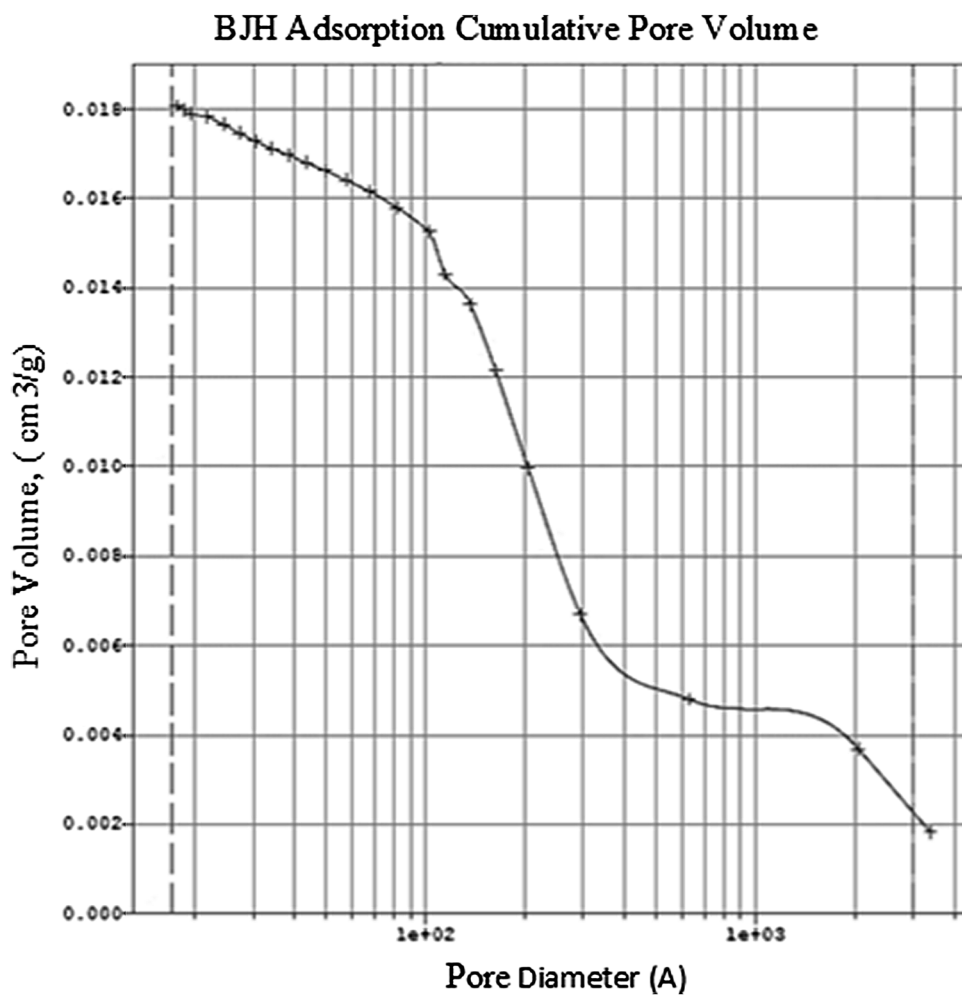
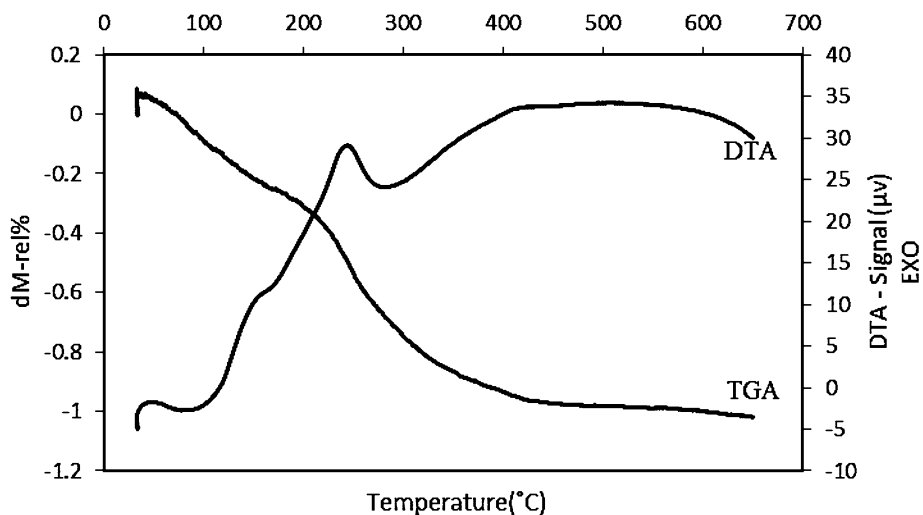


Fig. 7 TGA–DTA curve of the Fe/TiO₂



conditions in the blank were the same as the sample, but it had no catalyst. The concentration of phenol in the solution was measured using Beer–Lambert law and photo degradation of phenol was calculated using following equation:

$$\text{Degradation}\% = 100 \times [(A_{d_0} - A_d)/A_{d_0}] \quad (1)$$

where A_{d_0} and A_d are the absorbance of blank and sample, respectively [38].

H_2O_2

Adding proper amount of electron acceptor results in preventing the electron–hole recombination and increasing the number of hydroxyl radicals and other oxidizing agents. Optimization of H_2O_2 dosage is a fundamental factor in the photocatalytic degradation of phenol. Hydroxyl generation can be executed through three routes, the first route is H_2O_2 photo-dissociation, the second route is the reaction between H_2O_2 photogenerated electrons on TiO_2 surface, and the third one is the reaction between H_2O_2 and peroxy ion that is produced from the reaction of dissolved O_2 and electrons of conduction band [39]. An experiment was conducted with different dosages of H_2O_2 and the results are given in Fig. 8. It has been shown that at low H_2O_2 concentrations, the produced $\cdot OH$ radicals are not sufficient for phenol photocatalytic degradation. However, high concentrations of hydrogen peroxide will lead to a decrease in phenol degradation, since $\cdot OH$ radicals react with the excess H_2O_2 . This reaction consumes hydroxyl radicals and competes with phenol oxidation. According to Fig. 8, increasing the H_2O_2 dosage up to 12.5 ml enhances the activity of Fe/ TiO_2 and further increase will lead to lower efficiencies. Consequently, the optimum amount for H_2O_2 is 12.5 ml.

Air Bubbling

The role of aeration in photocatalytic degradation is inevitable. Dissolved oxygen (DO) increases quantum efficiencies of photocatalytic degradation partly by inhibiting electron–hole recombination. In fact, DO acts as electron acceptor during superoxide radical anion formation, which leads to separate electrons and holes. It has been reported that the reaction of O_2 with electrons at the surface of catalyst is slow and it is regarded as the rate-

determining step in photocatalysis. Air bubbling is the simplest way to supply molecular oxygen; moreover, it provides turbulence, which assists mass transfer [40, 41]. The effect of aeration on phenol degradation is displayed in Fig. 9. It is observed that after 120 min, When there is no oxidizing agent (no aeration, and no H_2O_2), phenol degradation is negligible. According to Fig. 9, increasing the aeration flow rate leads to enhance the phenol degradation. As a result, the highest flow rate (9 l/min) is considered the optimum. Albeit, it is of great importance that compared to H_2O_2 , aeration is less efficient.

Temperature

In general, the activation energy of photocatalytic reactions is provided by photons and operations take place at room temperature. To study the influence of temperature, an experiment was performed at 27, 37, and 47 °C. Figure 10 shows the effect of temperature rise on the photodegradation of phenol. It represents that the higher the temperature, the less phenol photodegradation. As it can be seen in Fig. 10 twenty degrees of temperature rise above room temperature drastically drops phenol degradation. In fact, degradation of phenol at 47 °C is inconsiderable. It could be the result of the decrease in dissolved oxygen at higher temperatures. Presence of oxygen is favorable and it prevents the recombination of e^- and h^+ of the Fe/ TiO_2 photocatalyst [42, 43]. Based on the obtained results, the catalytic degradation of phenol is recommended to be performed at ambient temperature.

Inorganic ions

The existence of inorganic ions is shown to have a significant effect on the photocatalytic degradation of organic

Fig. 8 The optimization of H_2O_2 dosage in the phenol degradation process

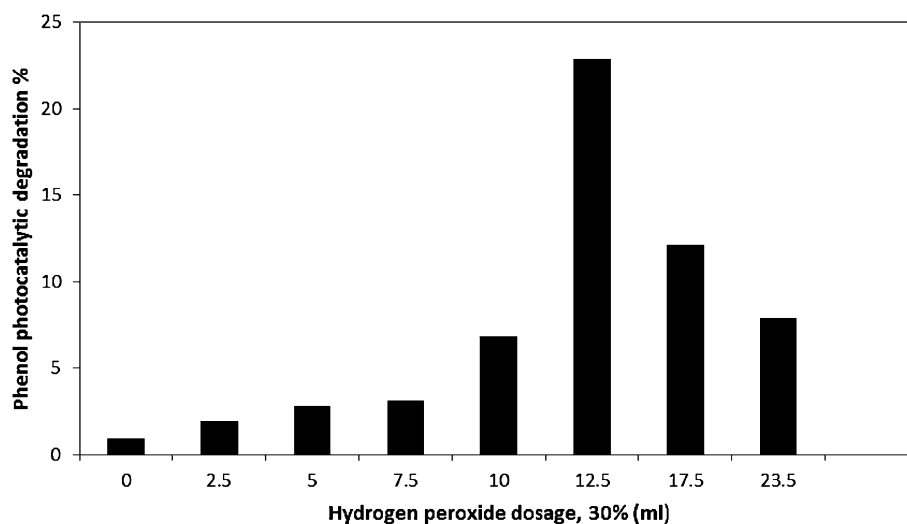


Fig. 9 The effect of aeration on phenol photodegradation

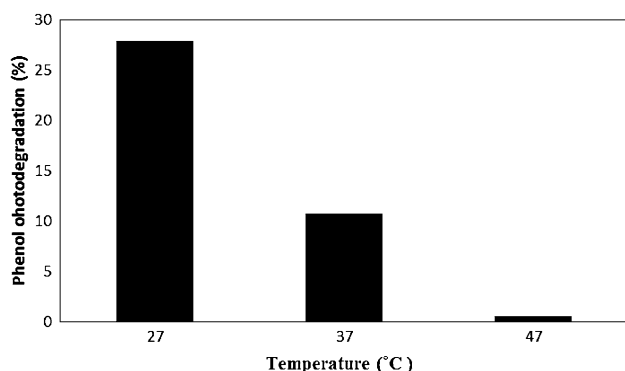
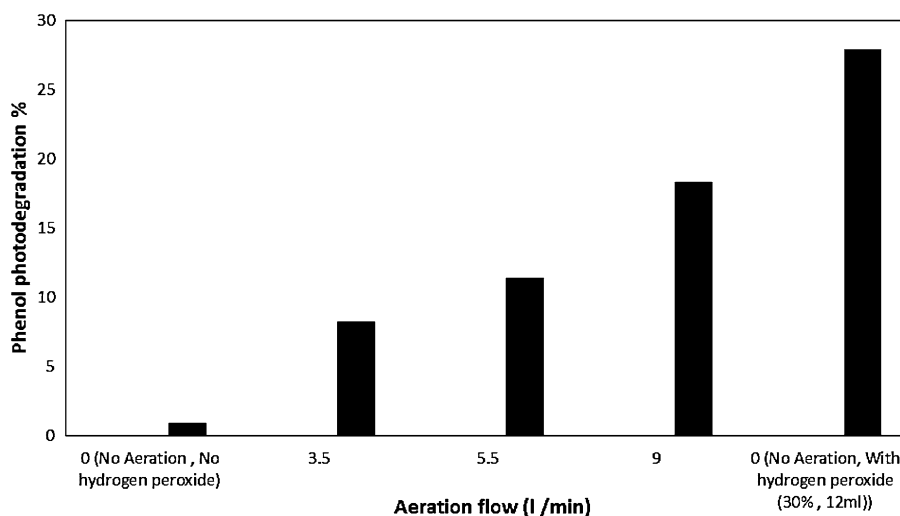


Fig. 10 The effect of temperature on phenol photodegradation

compounds. In this test, the effect of the existence of different inorganic ions including Ni^{3+} , Cu^{2+} , SO_4^{2-} , and Cl^- in the phenol synthetic wastewater was investigated. The concentration of additive ions was the same (1 mM) in each experiment. The results are shown in Fig. 11. Anions and phenol are in a competition to react with OH radicals, and thus they hinder phenol photodegradation. The low efficiency of the degradation process (less than 5 %) once SO_4^{2-} , and Cl^- being added to phenol solution highlights this finding. KASHIF Naeem and Ouyang Feng have enunciated that anions affect the phenol photocatalytic degradation, they reported the inhibition order of the investigated anions as $\text{Cl}^- > \text{SO}_4^{2-} > \text{NO}_3^- > \text{CO}_3^{2-}$ [44].

Cations absorbing on the surface of iron-modified titanium dioxide are reduced by activated electrons. Therefore, electron and holes will be separated more efficiently and their recombination is avoided. It seems that the existence of cations should have a positive influence on phenol degradation. Figure 11 shows that addition of copper

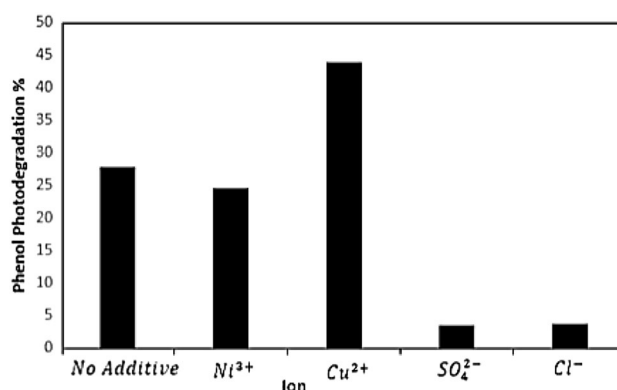


Fig. 11 The effect of existence of inorganic ions on the phenol photodegradation

enhances the performance of Fe/TiO_2 ; this arose from electron scavenging effect that inhibits the recombination of the photogenerated electron and holes. Whereas, the addition of Ni^{3+} slightly diminishes the efficiency of the catalyst, probably due to reaction with phenol and subsequently, the formation of phenol complexes. Accordingly, the influence of inorganic ions was observed to follow this order: $\text{Cu}^{2+} > \text{No additive} > \text{Ni}^{3+} > \text{Cl}^- > \text{SO}_4^{2-}$. Furthermore, it has been shown that the addition of copper as additive ion to phenol solution boosts the degradation of phenol; the highest phenol degradation efficiency after 120 min (43.85 %) was attained under this condition. From the observed superior performance of Fe/TiO_2 catalyst once copper ion was added to phenol synthetic wastewater, it can be concluded that the nanoparticles of Fe/TiO_2 will be an extremely capable catalyst for treating industrial wastewaters containing both phenol and heavy metals such as copper.

Conclusion

Iron-modified titanium dioxide was successfully synthesized by the sol–gel method. The outstanding results of the characterization of the catalyst are as follows: XPS results show that titanium and oxygen are the main elements, which are present in the surface of the catalyst. XRD results show that there are two peaks corresponding to the iron oxides of Fe₂O₃ in addition to the peaks belonging to rutile and anatase phases. This result indicates that iron is incorporated in TiO₂ lattice. Chemical composition of the catalyst by XRF declares that the ratio of (Fe₂O₃/TiO₂) is 0.21 %. The aggregated nanoparticles are observable in TEM images. Porosity of the catalyst is indicated in SEM image. BET calculation reveals that specific surface area of the catalyst is 5.1268 m²/g and average pore diameter is 13.9838 nm. Once, there is no oxidizing agent phenol degradation is inconsiderable. Experimental tests assert the positive effect of H₂O₂ addition and likewise the effect of aeration. The main objective of activity tests was focused upon the comparative evaluation of H₂O₂ addition and the application of Air Bubbling. Experimental results specified that the optimum amount for H₂O₂ dosage is 12.5 ml. It is notable that the effect H₂O₂ is more eminent. After 120 min, the degradation of phenol in an aerated reactor with the optimum flow rate was 18.26 %, while 27.87 % of phenol was decomposed in a system in the presence of proper amount of H₂O₂. Moreover, the existence of anions show inhibitory effect on the degradation of phenol, and the addition of cations such as Cu²⁺ into phenol solution exhibits a synergetic effect on the performance of the Fe/TiO₂. The temperature rise has adverse influence on the phenol photocatalytic degradation. Accordingly, temperatures higher than room temperature are not recommended.

Acknowledgments The financial support from University of Kurdistan is gratefully acknowledged.

Compliance with ethical standards

Conflict of interest The authors declare that they have no competing interests.

Open Access This article is distributed under the terms of the Creative Commons Attribution 4.0 International License (<http://creativecommons.org/licenses/by/4.0/>), which permits unrestricted use, distribution, and reproduction in any medium, provided you give appropriate credit to the original author(s) and the source, provide a link to the Creative Commons license, and indicate if changes were made.

References

- Watts, J.F., Wolstenholme, J.: An Introduction to Surface Analysis by XPS and AES. Copyright © 2003 by John Wiley & Sons Ltd, the Atrium, Southern Gate, Chichester, West Sussex PO19 8SQ, England
- Zhang, Q., Xu, L., Ning, P., Gu, J., Guan, Q.: Surface characterization studies of CuO–CeO₂–ZrO₂ catalysts for selective catalytic reduction of NO with NH₃. *Appl. Surf. Sci.* **317**, 955–961 (2014)
- Lorret, O., Francova, D., Waldner, G., Stelzer, N.: W-doped titania nanoparticles for UV and visible-light photocatalytic reactions. *Appl. Catal. B Environ.* **91**, 39–46 (2009)
- Lee, S.-Y., Park, S.-J.: TiO₂ photocatalyst for water treatment applications. *J. Ind. Eng. Chem.* **19**, 1761–1769 (2013)
- Karimi, L., Zohoori, S.: Superior photocatalytic degradation of azo dyes in aqueous solutions using TiO₂/SrTiO₃ nanocomposite. *J. Nanostruct. Chem.* **3**, 3–32 (2013)
- Park, H., Park, Y., Kim, W., Choi, W.: Surface modification of TiO₂ photocatalyst for environmental applications. *J. Photochem. Photobiol. C* **15**, 1–20 (2013)
- Sun, B., Vorontsov, A.V., Smirniotis, P.G.: Role of platinum deposited on TiO₂ in phenol photocatalytic oxidation. *Langmuir* **19**, 3151–3156 (2003)
- Fu, P., Zhang, P., Li, J.: Photocatalytic degradation of low concentration formaldehyde and simultaneous elimination of ozone by-product using palladium modified TiO₂ films under UV_{254+185nm} irradiation. *Appl. Catal. B Environ.* **105**, 220–228 (2011)
- Thomas, J., Yoon, M.: Facile synthesis of pure TiO₂ (B) nanofibers doped with gold nanoparticles and solar photocatalytic activities. *Appl. Catal. B Environ.* **111–112**, 502–508 (2012)
- Krejčíková, S., Matejová, L., Kocí, K., Obalová, L., Matej, Z., Capek, L., Šolcová, O.: Preparation and characterization of Ag-doped crystalline titania for photocatalysis applications. *Appl. Catal. B Environ.* **111–112**, 119–125 (2012)
- Wang, C.M., Heller, A., Gerischer, H.: Palladium catalysis of O₂ reduction by electrons accumulated on TiO₂ particles during photoassisted oxidation of organic compounds. *J. Am. Chem. Soc.* **114**, 5230–5234 (1992)
- Yao, Y., Ohko, Y., Sekiguchi, Y., Fujishima, A., Kubota, Y.: Self-sterilization using silicone catheters coated with Ag and TiO₂ nanocomposite thin film. *J. Biomed. Mater. Res. A* **85B**, 453–460 (2008)
- Wu, D., You, H., Jin, D., Li, X.: Enhanced inactivation of *Escherichia coli* with Ag-coated TiO₂ thin film under UV-C irradiation. *J. Photochem. Photobiol. A* **217**, 177–183 (2011)
- Yu, J., Xiong, J., Cheng, B., Liu, S.: Fabrication and characterization of Ag–TiO₂ multiphase nanocomposite thin films with enhanced photocatalytic activity. *Appl. Catal. B Environ.* **60**, 211–221 (2005)
- Angelis, F.D., Fantacci, S., Selloni, A., Nazeeruddin, M.K., Gratzel, M., Amer, J.: Time-dependent density functional theory investigations on the excited states of Ru(II)-dye-sensitized TiO₂ nanoparticles: the role of sensitizer protonation. *Chem. Soc.* **129**, 14156–14157 (2007)
- Morikawa, T., Ohwaki, T., Suzuki, K., Moribe, S., Kubota, S.T.: Visible-light-induced photocatalytic oxidation of carboxylic acids and aldehydes over N-doped TiO₂ loaded with Fe, Cu or Pt. *Appl. Catal. B Environ.* **83**, 56–62 (2008)
- Kay, A., Cesar, I., Gratzel, M.: New benchmark for water photooxidation by nanostructured α-Fe₂O₃ films. *J. Am. Chem. Soc.* **128**, 15714–15721 (2006)
- Sun, Q., Leng, W., Li, Z., Xu, Y.: Effect of surface Fe₂O₃ clusters on the photocatalytic activity of TiO₂ for phenol degradation in water. *J. Hazard. Mater.* **229**, 224–232 (2012)
- Zhang, Y., Li, Q.: Synthesis and characterization of Fe-doped TiO₂ films by electrophoretic method and its photocatalytic activity toward methyl orange. *Solid State Sci.* **16**, 16–20 (2013)
- Palanisamy, B., Babu, C.M., Sundaravel, B., Anandan, S., Murugesan, V.: Sol–gel synthesis of mesoporous mixed Fe₂O₃/



- TiO₂ photocatalyst: application for degradation of 4-chlorophenol. *J. Hazard. Mater.* **252–253**, 233–242 (2013)
21. Ni, M., Leung, M.K.H., Leung, D.Y.C., Sumathy, K.: A review, and recent developments in photocatalytic water-splitting using TiO₂ for hydrogen production. *Renew. Sustain. Energy Rev.* **11**, 401–425 (2007)
 22. Iliev, V., Tomova, D., Rakovsky, S.: Nanosized N-doped TiO₂, and gold modified semiconductors—photocatalysts for combined UV–visible light destruction of oxalic acid in aqueous solution. *Desalination* **260**, 101–106 (2010)
 23. Oganisian, K., Hreniak, A., Sikora, A., Gaworska-Koniarek, D., Iwan, A.: Synthesis of iron doped titanium dioxide by sol–gel method for magnetic applications. *Process. Appl. Ceram.* **9**, 43–51 (2015)
 24. Hreniak, A., Gryzlo, K., Boharewicz, B., Sikora, A., Chmielowiec, J., Iwan, A.: Preparation and optical properties of iron-modified titanium dioxide obtained by sol–gel method. *Opt. Mater.* **46**, 45–51 (2015)
 25. Ranjit, K., Viswanathan, B.: Synthesis, characterization and photocatalytic properties of iron-doped TiO₂ catalysts. *J. Photochem. Photobiol. A Chem.* **108**, 79–84 (1997)
 26. Liu, Y., Wei, J.H., Xiong, R., Pan, C.X., Shi, J.: Enhanced visible light photocatalytic properties of Fe-doped TiO₂ nanorod clusters and monodispersed nanoparticles. *Appl. Surf. Sci.* **257**, 8121–8126 (2011)
 27. Naik, B., Parida, K.M.: Solar light active photodegradation of phenol over a Fe_xTi_{1-x}O_{2-y}N_y nanophotocatalyst. *Ind. Eng. Chem. Res.* **49**, 8339–8346 (2010)
 28. Barakata, N.A.M., Taha, A., Motlak, M., Nassar, M.M., Mahmoud, M.S., Al-Deyab, S.S., El-Newehy, M., Kim, H.Y.: ZnO & Fe₂O₃-incorporated TiO₂ nanofibers as super effective photocatalyst for water splitting under visible light radiation. *Appl. Catal. A Gen.* **481**, 19–26 (2014)
 29. Schicks, J., Neumann, D., Specht, U., Vesper, G.: Nanoengineered catalysts for high-temperature methane partial oxidation. *Catal. Today* **81**, 287–296 (2003)
 30. De Biasi, R.S., Grillo, M.L.N.: ESR investigation of Fe³⁺ diffusion in rutile. *J. Phys. Chem. Solids* **57**, 137–138 (1996)
 31. Zhu, Jiefang, Chen, Feng, Zhang, Jinlong: Fe³⁺-TiO₂ photocatalysts prepared by combining sol–gel method with hydrothermal treatment and their characterization. *J. Photochem. Photobiol. A* **180**, 196–204 (2006)
 32. Egerton, T.A., Harris, E., Lawson, E.J., Mile, B., Rowlands, C.C.: An EPR study of diffusion of chromium into rutile. *Phys. Chem. Chem. Phys.* **2**, 3275–3281 (2000)
 33. Wanger, C.D., Riggs, W.M., Davis, L.E., Moulder, J.F.: *Handbook of X-ray Photoelectron Spectroscopy*. Eden Prairie, Minnesota (1979)
 34. Pang, Y.L., Abdullah, A.Z.: Effect of low Fe³⁺ doping on characteristics, photocatalytic activity and reusability of TiO₂ nanotubes catalysts for removal of Rhodamine B from water. *J. Hazard. Mater.* **235–236**, 326–335 (2012)
 35. Yuan, R., Zhou, B., Hua, D., Shi, C.: Enhanced photocatalytic degradation of humic acids using Al and Fe co-doped TiO₂ nanotubes under UV/ozonation for drinking water purification. *J. Hazard. Mater.* **262**, 527–538 (2013)
 36. Leofanti, G., Padovan, M., Tozzola, G., Venturelli, B.: Surface area and pore texture of catalysts. *Catal. Today* **41**, 207–219 (1998)
 37. Mesgari, Z., Gharagozloub, M., Khosravi, A., Gharanjig, K.: Synthesis, characterization and evaluation of efficiency of new hybrid Pc/Fe–TiO₂ nanocomposite as photocatalyst for decolorization of methyl orange using visible light irradiation. *Appl. Catal. A Gen.* **411–412**, 139–145 (2012)
 38. Akhlaghian, F., Sohrabi, S.: Fe/TiO₂ catalyst for photodegradation of phenol in water. *Int. J. Eng. (IJE) Trans. A Basics* **28**, 499–506 (2015)
 39. Luenloi, T., Chalermssinsuwan, B., Sreethawong, T., Hinchiranan, N.: Photodegradation of phenol catalyzed by TiO₂ coated on acrylic sheets: kinetics and factorial design analysis. *Desalination* **274**, 192–199 (2011)
 40. Youn, N.K., Heo, J.E., Joo, O.S., Lee, H., Kim, J., Min, B.K.: The effect of dissolved oxygen on the 1,4-dioxane degradation with TiO₂ and Au–TiO₂ photocatalysts. *J. Hazard. Mater.* **177**, 216–221 (2010)
 41. Ling, C.M., Mohamad, A.R., Bhatia, S.: Performance of photocatalytic reactors using immobilized TiO₂ film for the degradation of phenol and methylene blue dye present in water stream. *Chemosphere* **57**, 547–554 (2004)
 42. Nezamzadeh-Ejehieh, A., Salimi, Z.: Heterogeneous photodegradation catalysis of o-phenylenediamine using CuO/X zeolite. *Appl. Catal. A Gen.* **390**, 110–118 (2010)
 43. Ahmed, S., Rasul, M.G., Martens, W.N., Brown, R., Hashib, M.A.: Heterogeneous photocatalytic degradation of phenols in wastewater: a review on current status and developments. *Desalination* **261**, 3–18 (2010)
 44. Kashif, N., Ouyang, F.: Parameters effect on heterogeneous photocatalysed degradation of phenol in aqueous dispersion of TiO₂. *J. Environ. Sci.* **21**, 527–533 (2009)